Crystal structure, Hirshfeld surface analysis and DFT calculation of *N,N'*-(1,4-phenylenebis(methanylylidene))bis(4-fluoroaniline)

Yada Muangkaew[a], Wikorn Punyain[a] and Kittipong Chainok[b]*

[a]Department of Chemistry, Faculty of Science, Naresuan University, Muang, Phitsanulok, 65000, Thailand
[b]Materials and Textile Technology, Faculty of Science and Technology, Thammasat University, Khlong Luang, Pathum Thani, 12121, Thailand
*Corresponding author. E-mail: kc@tu.ac.th

ABSTRACT

In the title Schiff base compound, $C_{20}H_{14}F_2N_2$ [systematic name: *N,N'*-(1,4-phenylenebis(methanylylidene))bis(4-fluoroaniline)] was synthesized by condensation reaction of 1,4-benzenedicarboxaldehyde and 4-fluoroaniline and was crystallized in the centrosymmetric monoclinic space group $P2_1/c$. X-ray structure was revealed a non-planar molecule because the two dihedral angles of mean plane of the central benzene ring with each of terminal fluorobenzene rings were 51.33(6)° and 52.49(6)°. The molecular crystal was linked together by a combination types I and II, i.e. F···F, C-H···F, C-H···N and C-H···π interactions, forming a three-dimensional supramolecular structure. The Hirshfeld surface analysis indicates a high percentage of C···H/H···C (41.1%) contacts in the crystal. The molecular structures are optimized using density functional theory (DFT) at B3LYP/6–311G(*d*) level and compared with the experimentally determined in the solid state.

Keywords: crystal structure, DFT, Hirshfeld surface analysis, hydrogen bonds, halogen bonds, Schiff base

INTRODUCTION

Schiff base compounds consist of any imine groups that containing C=N bond, showing the interested biological activities, such as have attracted considerable interest due to their important biological activities such as antibacterial (Kaczmarek *et al.*, 2018), antifungal (Lam *et al.*, 2016) and anti-inflammatory (Adsule *et al.*, 2006). Schiff base ligands can be used as building blocks in metallosupramolecular complex synthesis in which showing magnetic spin crossover (Létard *et al.*, 1997, 1998) and luminescence properties (Kawamoto *et al.*, 2008). They are also convenient model compounds for study theoretical aspects in architectural molecules by means of molecular motifs formation by supramolecular interactions. In this report, we aim to synthesize, X-ray structure analysis, structural analysis and DFT computational calculations of the title new Schiff base compound containing the fluorobenzene groups, $C_{20}H_{14}F_2N_2$. Moreover, Hirshfeld surface analysis was used to investigate the intermolecular contacts and weak contributions involved in the supramolecular stabilization.

EXPERIMENTAL

Synthesis of *N,N*'-[(1,4-phenylenebis(methanylylidene))bis(4-fluoroaniline)]
At room temperature, 1,4-benzenedicarboxaldehyde (2,70 ml, 0.02 mol) was added
to a benzene solution (100 ml) of 4-fluoroaniline (4.45 g, 0.04 mol), with a few
drops of acetic acid added as catalyst. The reaction mixture was stirred under reflux
at 110 °C. After 6 h of reflux, the yellow solution was neutralized with Na_2CO_3 (2
mmol), filtered, and concentrated to dryness in vacuum. The suitable crystals for
single crystal X-ray diffraction analysis were obtained by recrystallized the yellow
precipitate of Schiff base product by using yellow precipitate of Schiff base product
by using residue product of the title compound from a mixture of dichloromethane
and petroleum ether (2:1, v/v).

X-ray crystallography
Crystal data, data collection and structure refinement details are summarized in
Table 1. All H atoms were positioned geometrically with C–H = 0.93 Å and
refined with using a riding model with $U_{iso}(H) = 1.2U_{eq}(C)$.

RESULTS AND DISCUSSION

Structural commentary
As shown in Fig. 1, the molecular structure of this fluorobenzene Schiff base
compound was not a planar molecule. The central benzene ring made dihedral
angles to 51.33(6)° with C1-C6 fluorobenzene ring and, to 52.49(6)° with the
another C15-C20 fluorobenzene ring, with the outer fluorobenzene rings C1–C6 and
C15–C20, respectively, while the dihedral angle between the two fluorobenzene
rings was 3.92 (5)°. The both imine bonds, C7-N1 and C14-N2, was 1.262(2) Å and
1.268(2) Å respectively, confirmed their significant C=N imine bond character. All
bond lengths and angles are normal and comparable to those observed in similar
crystal structures (W.H.Ojala, B.Balidemaj, J.A.Johnson, S.N.Larson, C.R.Ojala
(2014) CrystEngComm ,16,7226).
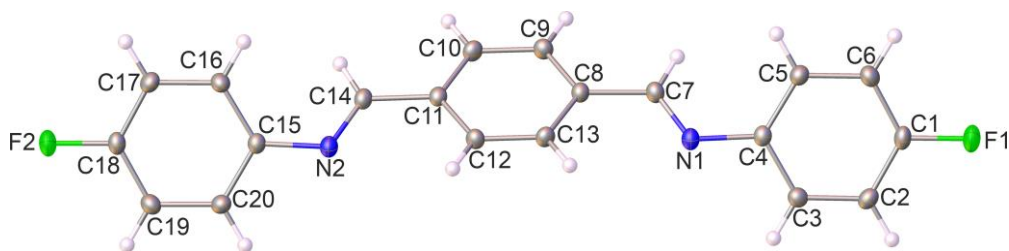
Figure 1
X-ray structure of the title Schiff base compound with atomic labelling.
Displacement ellipsoids are drawn at the 40% probability level.

Supramolecular features

In the molecular crystal, molecules were linked by type-I F···F halogen bonds (Ramasubbu *et al*., 1986) [C1–F1···F2–C18$^{(i)}$ = 3.005(2) Å, C1–F1···F2–C18$^{(ii)}$ = 3.012(2) Å; Symmetry codes (i) *x*–1, 1/2–*y*, *z*–1/2; (ii) *x*–1, 3/2–*y*, *z*–1/2] and weak C–H···F hydrogen bonds as shown in Table 2, forming a two-dimensional layer structure along the *a* axis as shown in Fig. 2. Several intermolecular weak C–H···F hydrogen bonds as shown in Table 2, edge to face as C–H···π interactions are observed in the crystal structure as shown in Fig. 3 and Table 2. Furthermore, weak interactions along with C-H···N hydrogen bond and halogen bond type-II were [C18–F2···F2–C18$^{(iii)}$ = 3.220 (3) Å; Symmetry code (iii) *x*–1, 1/2–*y*, *z*–1/2; *x*–1, 3/2–*y*, *z*–1/2] are further linked the adjacent layers into a three-dimensional supramolecular structure.
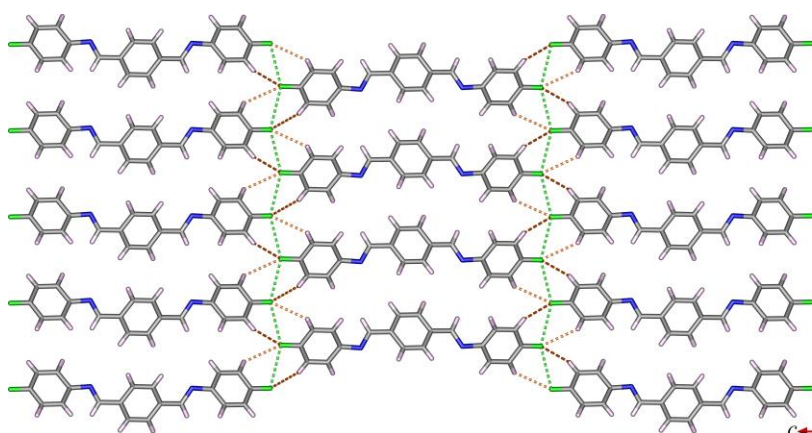
Figure 2

A view of the two-dimensional supramolecular layer structure formed by C-H···F hydrogen bonds (orange dashed lines, Table 1) and type-I F···F halogen bonds (green dashed lines) in the crystal of the title compound, propagating along the *a*-axis direction.
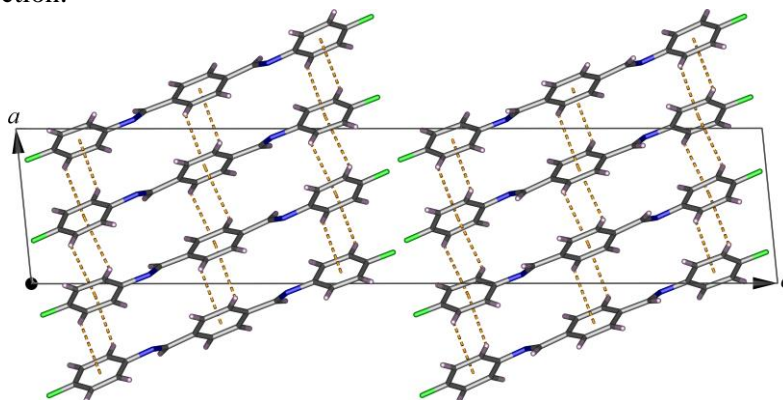
Figure 3

The crystal packing of the title compound along the b axis, showing weak C-H···π interactions (orange dashed lines, Table 1).

Table 1 Hydrogen-bond geometry (Å, °) Cg1, Cg2 and Cg3 are the centroids of the C1-C6, C8-C13 and C15-C20 rings, respectively.

$D-\text{H}\cdots A$	$D-\text{H}$	$\text{H}\cdots A$	$D\cdots A$	$D-\text{H}\cdots A$
C2—H2···F2[i]	0.93	2.85	3.445 (2)	122.8
C3—H3···Cg3[ii]	0.93	2.81	3.519 (2)	133.3
C6—H6···F2[iii]	0.93	2.73	3.412 (2)	130.6
C6—H6···Cg3[iv]	0.93	2.92	3.605 (2)	130.5
C9—H9···Cg2[v]	0.93	2.99	3.579 (2)	125.1
C16—H16···N1[ii]	0.93	2.75	3.524 (2)	141.1
C17—H17···F1[vi]	0.93	2.74	3.419 (2)	130.7
C17—H17···Cg1[ii]	0.93	2.86	3.504 (2)	132.8
C19—H19···F1[vii]	0.93	2.86	3.440 (2)	121.4
C20—H19···Cg1[iv]	0.93	2.97	3.593 (2)	126.7

Symmetry codes: (i) $x-1$, $-y+3/2$, $z-1/2$; (ii) $-x+2$, $y+1/2$, $-z+3/2$; (iii) $x-1$, $-y+1/2$, $z-1/2$; (iv) $-x+1$, $y-1/2$, $-z+3/2$; (v) $-x+2$, $y-1/2$, $-z+3/2$; (vi) $x+1$, $-y+3/2$, $z+1/2$; (vii) $x+1$, $-y+1/2$, $z+1/2$.

Hirshfeld surface analysis

Hirshfeld surfaces analysis with their two-dimensional fingerprints has been a very useful tool for visualization and comparison on a simple coloring scheme of intermolecular interactions in crystal structures which were relative to van der Waals radii (Spackman & Jayatilaka, 2009), and was carried out by using Crystal Explorer 17.5 (Turner *et al.*, 2017). The red and blue colors are used for shorter and longer contacts, respectively, while white highlights used for contacts around the van der Waals separations. Complementary regions are visible in the fingerprint plots of (d_e, d_i) pairs, where d_e is the distance from a point on the Hirshfeld surface to the nearest external atom, and d_i is the distance from the same point on the Hirshfeld surface to the nearest atom internal to the surface. All C–H···π, C–H···N and C–H···F contacts are recognized in the shape-index surface as a combination of pale orange and bright-red sports depression areas in Fig. 4.
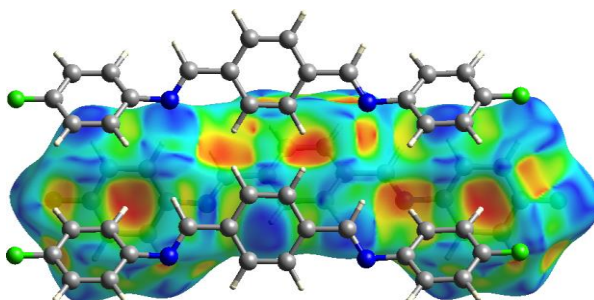
Figure 4
Hirshfeld surfaces for the title compound, showing shape-index with the pale-orange spots indicating the involvement of the C-H···π interactions.

The two-dimensional fingerprint plots were illustrated the difference between the intermolecular interaction patterns. As can be seen from Fig. 5, the H···C/C···H contacts, corresponding to the C–H···π interactions appear to be the major contributor to the Hirshfeld surface (comprise 41.1%), showing two distinct spikes with 3.4Å of $d_e + d_i$ summation. Other significant contributions to the surfaces are also made by H···F/F···H contacts, corresponding to weak C–H···F interactions (comprise 15.7%) and appeared as the broad green spikes in the middle region of the fingerprint plots with 2.8Å of $d_e + d_i$ summation. The remaining contributions were distributed among F···F, N···H/H···N and H···H contacts in which the largest contributor to the Hirshfeld surfaces were H···H interactions (comprise 30.5%) with 2.4Å of de + di summation.
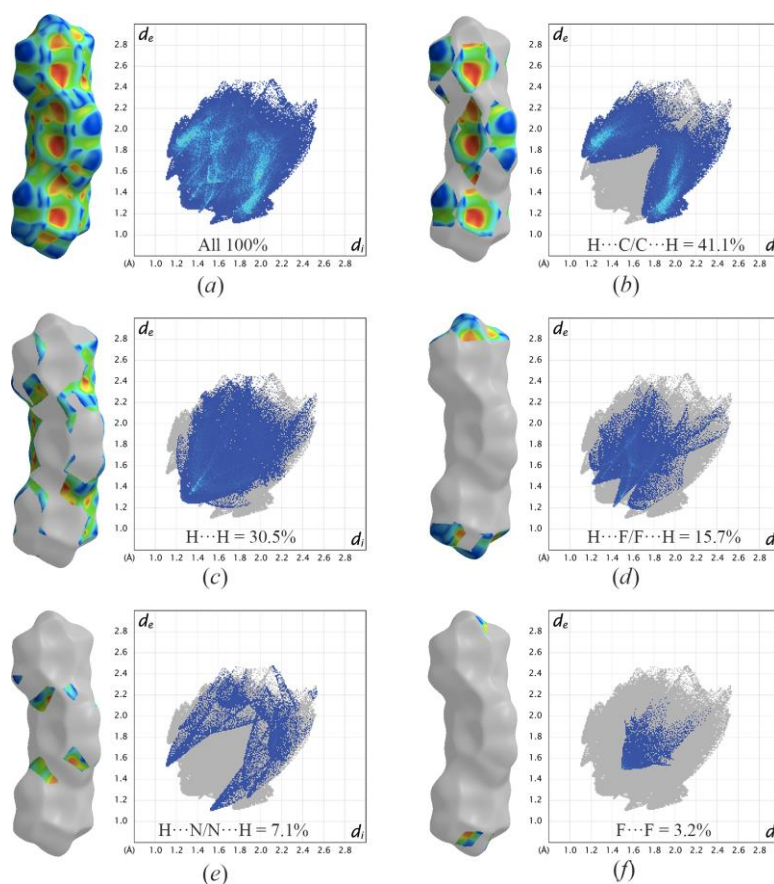
Figure 5
The two-dimensional fingerprint plot for the title compound, delineated into (a) all interactions, (b) H···C/C···H, (c) H···H, (d) H···F/F···H, (e) H···N/N···H and (f) F···F interactions; shape index surfaces for each plot, indicating the relevant surface patches associated with the specific contacts, are shown on the left.

Theoretical calculations

To support the experimental data based on the basis of the X-ray diffraction studying, DFT calculations were performed using the GAUSSIAN09 software package (Frisch et al., 2009). Full geometry optimizations were calculated using B3LYP level of theory with a 6–311G(d) basis set. The optimized parameters such as bond lengths and angles were in generally good agreement with the experimental crystallographic data, Table 3. The calculated torsion angles for C5–C4–N1–C7 and C20–C15–N2–C14 were -146.1° and 144.7°, respectively, whereas the corresponding torsion angles for the experimental data were -144.4 (2) ° and 142.5 (2)°, respectively. The slight deviations from the experimental values were different optimization condition. Based on GAUSSIAN09 calculation was performed in an isolated condition, whereas the crystal environment and intermolecular interactions affect the results of the three-dimensional network structure from X-ray diffraction data.

Table 2 Experimental and calculated bond lengths (Å)

Bond	X-ray	B3LYP/6-311G(d)	Difference
F1-C1	1.353 (2)	1.352	0.001
F2-C18	1.357 (2)	1.352	0.005
N1-C4	1.419 (2)	1.404	0.015
N1-C7	1.262 (2)	1.277	-0.015
N2-C14	1.268 (2)	1.277	-0.009
N2-C15	1.420 (2)	1.404	0.016
C1-C2	1.375 (2)	1.388	-0.013
C1-C6	1.374 (2)	1.387	-0.013
C2-C3	1.382 (2)	1.391	-0.009
C3-C4	1.395 (2)	1.403	-0.008
C4-C5	1.392 (2)	1.404	-0.012
C5-C6	1.383 (2)	1.391	-0.008
C7-C8	1.468 (2)	1.466	0.002
C8-C9	1.389 (2)	1.400	-0.011
C8-C13	1.399 (2)	1.408	-0.009
C9-C10	1.382 (2)	1.390	-0.008
C10-C11	1.393 (2)	1.400	-0.007
C11-C12	1.394 (2)	1.408	-0.014
C11-C14	1.469 (2)	1.466	0.003
C12-C13	1.375 (2)	1.381	-0.006
C15-C16	1.392 (2)	1.404	-0.012
C15-C20	1.391 (2)	1.403	-0.012
C16-C17	1.384 (2)	1.391	-0.007
C17-C18	1.374 (2)	1.387	-0.014
C18-C19	1.372 (2)	1.388	-0.016
C19-C20	1.382 (2)	1.389	-0.007

Table 3 Experimental details

Crystal data	
Chemical formular	$C_{20}H_{14}F_2N_2$
M_r	320.33
Crystal system, Space group	Monoclinic, $P2_1/c$
Temperature (K)	296
a, b, c (Å)	7.5520 (8), 5.7560 (6), 36.291 (4)
β (°)	95.710 (4)
V (Å^3)	1569.7 (3)
Z	4
Radiation type	Mo $K\alpha$
μ (mm^{-1})	0.10
Crystal size (mm)	$0.36 \times 0.35 \times 0.26$
Data collection	
Diffractometer	Bruker D8 QUEST CMOS
Absorption correction	Multi-scan
	SADABS2014/4 (Bruker,2014/4) was used for absorption correction. wR2(int) was 0.0672 before and 0.0565 after correction. The Ratio of minimum to maximum transmission is 0.9474. The λ/2 correction factor is 0.00150.
T_{min}, T_{max}	0.707, 0.746
No. of measured, independent and observed [$I > 2\sigma(I)$] reflections	70251, 3905, 2762
R_{int}	0.043
$(\sin\theta/\lambda)_{max}$ (Å^{-1})	0.668
Refinement	
$R[F^2 > 2\sigma(F^2)]$, $wR(F^2)$, S	0.053, 0.157, 1.06
No. of reflections	3905
No. of parameters	218
H-atom treatment	H-atom parameters constrained
$\Delta\rho_{max}$, $\Delta\rho_{min}$ (e Å^{-3})	0.27, −0.19

Computer programs: *APEX* 3 (Bruker, 2016), *SAINT* V8.38A (Bruker, 2016), ShelXT (Sheldrick, 2015a), *SHELXL* (Sheldrick, 2015b), Olex2 (Dolomanov *et al.*, 2009).

CONCLUSIONS

In this work, we are successfully obtained the monoclinic crystal structure of N,N'-(1,4-phenylenebis(methanylylidene))bis(4-fluoroaniline) with $P2_1/c$ space group. The two fluorobenzene rings were twist from the central benzene ring around 50 degrees caused its X-ray structure being non-planar. Their molecular motifs were packed together by the C–H···F, F···F interactions, and substantially major C–H···π interactions between the layers being a mainly role of the crystal packing corresponding to Hirshfeld surfaces calculation. DFT calculations at B3LYP/6–311+G(d) level of theory was resulted optimized parameters of structural geometry corresponding well with the results from X-ray crystallographic data.

REFERENCES

Adsule, S., Barve, V., Chen, D., Ahmed, F., Dou, Q. P., Padhye, S. & Sarkar, F. H. (2006). Novel Schiff base copper complexes of quinoline-2 carboxaldehyde as proteasome inhibitors in human prostate cancer cells. *J. Med. Chem.* **49**, 7242–7246

Dolomanov, O. V., Bourhis, L. J., Gildea, R. J., Howard, J. A. K. & Puschmann, H. (2009). OLEX2: a complete structure solution, refinement and analysis program. *J. Appl. Cryst.* 42, 339–341.

Frisch, M. J., *et al.* (2009). *GAUSSIAN09*. Gaussian Inc., Wallingford, CT, USA

Kaczmarek, M. T., Zabiszak, M., Nowak, M. & Jastrzab, R. (2018). Lanthanides: Schiff base complexes, applications in cancer diagnosis, therapy, and antibacterial activity. *Coord. Chem. Rev.* **370**, 42–54.

Kawamoto, T., Nishiwaki, M., Tsunekawa, Y., Nozaki, K. & Konno, T. (2008). Synthesis and Characterization of Luminescent Zinc(II) and Cadmium(II) Complexes with N,S-Chelating Schiff Base Ligands. *Inorg. Chem.* **47**, 3095–3104.

Lam, P.-L., Lee, K. K.-H., Kok, S. H.-L., Gambari, R., Lam, K.-H., Ho, C.-L., Ma, X., Lo, Y.-H., Wong, W.-Y., Dong, Q.-C., Bian, Z.-X. & Chui, C.-H. (2016). Antifungal study of substituted 4-pyridylmethylene-4′-aniline Schiff bases. *RSC Adv.* **6**, 104575–104581.

Létard, J.-F., Guionneau, P., Codjovi, E., Lavastre, O., Bravic, D., Chasseau, D. & Kahn, O. (1997). Wide Thermal Hysteresis for the Mononuclear Spin-Crossover Compound *cis*-Bis(thiocyanato)bis[*N*-(2'-pyridylmethylene)-4-(phenylethynyl)anilino]iron(II). *J. Am. Chem. Soc.* **119**, 10861–10862.

Létard, J.-F., Guionneau, P., Rabardel, L., Howard, J. A. K., Goeta, A. E., Chasseau, D. & Kahn, O. (1998). Structural, Magnetic, and Photomagnetic Studies of a Mononuclear Iron(II) Derivative Exhibiting an Exceptionally Abrupt Spin Transition. Light-Induced Thermal Hysteresis Phenomenon. *Inorg. Chem.* **37**, 4432–4441.

Ramasubbu, N., Parthasarathy, R. & Murray-Rust, P. (1986). Angular preferences of intermolecular forces around halogen centers: preferred directions of approach of electrophiles and nucleophiles around carbon-halogen bond. *J. Am. Chem. Soc.* **108**, 4308–4314.

Sheldrick, G. M. (2015*a*). *SHELXT* – Integrated space-group and crystal-structure
      determination. *Acta Cryst.* A**71**, 3–8.

Sheldrick, G. M. (2015*b*). Crystal structure refinement with *SHELXL. Acta Cryst.* C**71**, 3–8.

Spackman, M. A. & Jayatilaka, D. (2009). Hirshfeld surface analysis. *CrystEngComm*, **11**,
      19–32.

Turner, M. J., McKinnon, J. J., Wolff, S. K., Grimwood, D. J., Spackman, P. R., Jayatilaka,
      D. & Spackman, M. A. (2017). CrystalExplorer17. The University of Western
      Australia.